Membrane Water Treatment, *Vol. 6*, *No. 4* (*2015*) *309-321*
DOI: http://dx.doi.org/10.12989/mwt.2015.6.4.309

Synthesis and characterization of polyamide thin-film nanocomposite membrane containing ZnO nanoparticles

A.S. AL-Hobaib [1], Jaber El Ghoul [*2,3] and Lassaad El Mir [2,3]

[1] *Institute of Atomic Energy Research*, *King Abdulaziz City for Science and Technology* (*KACST*), *11442 P.O. Box 6086 Riyadh*, *Saudi Arabia*
[2] *Al Imam Mohammad Ibn Saud Islamic University* (*IMSIU*), *College of Sciences*, *Department of Physics*, *Riyadh 11623*, *Saudi Arabia*
[3] *Laboratory of Physics of Materials and Nanomaterials Applied at Environment* (*LaPhyMNE*), *Gabes University*, *Faculty of Sciences of Gabes*, *6072*, *Tunisia*

(*Received December 24*, *2014*, *Revised March 26*, *2015*, *Accepted April 04*, *2015*)

Abstract. We report in this study the synthesis of mixed matrix reverse osmosis membranes by interfacial polymerization (IP) of thin film nanocomposite (TFNC) on porous polysulfone supports (PS). This paper investigates the synthesis of ZnO nanoparticles (NPs) using the sol-gel processing technique and evaluates the performance of mixed matrix membranes reached by these aerogel NPs. Aqueous m-phenyl diamine (MPD) and organic trimesoyl chloride (TMC)-NPs mixture solutions were used in the IP process. The reaction of MPD and TMC at the interface of PS substrates resulted in the formation of the thin film composite (TFC). NPs of ZnO with a size of about 25 nm were used for the fabrication of the TFNC membranes. These membranes were characterized and evaluated in comparison with neat TFC ones. Their performances were evaluated based on the water permeability and salt rejection. Experimental results indicated that the NPs improved membrane performance under optimal concentration of NPs. By changing the content of the filler, better hydrophilicity was obtained; the contact angle was decreased from 74° to 32°. Also, the permeate water flux was increased from 26 to 49 L/m2.h when the content of NPs is 0.1 (wt.%) with the maintaining of lower salt passage of 1%.

Keywords: *Nano*-ZnO; interfacial polymerization; nanocomposite; nanofiltration; desalination

1. Introduction

The growing demand for fresh water and the remarkable water crisis have spurred enormous interest in energy efficient technologies to produce safe drinking water from the ocean. Membrane filtration based on reverse osmosis (RO) is one of the most promising ways to desalinate seawater or brackish water, and thin film composite (TFC) membranes, comprised of ultra-thin active layers upon porous supports, have been widely used for this application (Peterson 1993,Wilf 2007). Due to their completely hydrophilic characteristic and their certain functionality to benefit membrane properties of fouling reduction, inorganic materials incorporation into the polymer matrix is being of great interest (Wang *et al*. 2011). Recently, extensive efforts are being devoted to incorporate

*Corresponding author, Assistant Professor, E-mail: ghoultn@yahoo.fr

http://www.techno-press.org/?journal=mwt&subpage=7 ISSN: 2005-8624 (Print), 2092-7037 (Online)

inorganic nanoparticles into polymeric membrane. It has been proved that inorganic materials could be incorporated, by using doping and coating technologies, into membranes (Kwak *et al*. 2001, Cornrlius *et al*. 2001). However, the coating technology imposes the problems of the instability of inorganic materials onto polymer surface, especially for those not subject to chemical bonds or physical restraints between the inorganic materials and membrane matrix. On the other hand, the doping technology has the disadvantage that inorganic materials are buried in the polymer matrix and in turn rendered non-functional. The concept for formation of mixed matrix reverse osmosis membranes has been reported by interfacial polymerization of nanocomposite thin films on porous supports (Jeong *et al*. 2007). The progression of nano-technology in membrane materials science has provided an attractive alternative to polymeric materials (Vaishali *et al*. 2014, Xie *et al*. 2012, Mercy *et al*. 2014).

By applying an in-situ interfacial polymerization procedure, titanium oxide nanoparticles have been incorporated into polyamide (PA) thin film membranes (Lee *et al*. 2008). It has been shown a significant improvement in fouling resistance within polyethersulfone-TiO_2 nanoparticles composite membranes made from casting solution consisting of various compositions of polymer solvents (DMF and EtOH) and additive TiO_2 (Sotto *et al*. 2011). Silica oxide nanoparticles have been incorporated into PA thin film membrane via in-situ interfacial polymerization process (Jadav and Singh 2009). Zeolite nano-particles have been used to prepare nanocomposite membrane where first zeolite nano-particles are synthesized via a template hydrothermal reaction followed by a series of complex processes involving template removal, carbonization, sodium exchange and calcinations (Lind *et al*. 2009). Membranes of polyvinylidene fluoride were prepared using zirconia as the bulk material (Bottino *et al*. 2000). With the addition of ZnO, polyethersulfone membranes were synthesized by diffusion induced phase inversion in N-methylpyrrolidone. It should be pointed that the membrane materials reached by ZnO nanoparticles have significantly improvements. Due to a higher hydrophilicity of the ZnO, membranes showed lower flux decline and better permeability compared to neat polymeric membrane. ZnO nanoparticles provide a remarkable improvement in the methylene blue rejection potential (Saleh and Gupta 2012). Aluminum oxide (Al_2O_3) nanoparticles were also incorporated into a membrane of polyvinylidene fluoride using dimethyl acetamide as solvent (Liu *et al*. 2011). A same type of polymer was used to prepare a membrane by doping with anhydrous and hydrated aluminum oxide particles through in-situ particles embedment and subsequent crystal growth under a hydrothermal environment (Wang *et al*. 2011).

The increase of the surface to volume ratio obtained when ZnO is used as particles in a nano-sized scale and the lower cost of ZnO make this alternative a potential system that can meet the demand of an efficient and lower-cost device. Due to its excellent optical, electrical, mechanical and chemical properties, ZnO is one of the most important multifunctional semiconductor materials and exceptionally important for application in photo-catalysis and anti-bacterial materials (El Ghoul *et al*. 2013, Omri *et al*. 2013, Hu *et al*. 2010). Furthermore, another big problem that can limit the application of nanoparticles, is their toxicity since it is thought that nanoparticles may persist as small particles in aquatic systems and that their bioavailability could be significantly greater than that of larger particles. The studies conducted on the ZnO nanoparticles show positive results (Yuan *et al*. 2010, Berardis *et al*. 2010, Song *et al*. 2010). Since the size distribution and surface area are not related to toxicity, the use of ZnO nanoparticles does not produce an increase in toxicity. By comparison of the toxicity in algae of nanoparticles ZnO, bulk ZnO and $ZnCl_2$, Franklin *et al*. have observed that toxicity is attributable solely to dissolved zinc, this is, to simple solubility of the compounds since ZnO nanoparticles

aggregate in freshwater systems forming flocks of even several microns with a saturation solubility similar to that of bulk ZnO (Franklin *et al*. 2007). Also, since ZnO nanoparticles will be embedded in a solid matrix (the membrane), a stable system can be developed, keeping their physical properties associated to their size and the chemical activity related to their availability in the membrane. Thus, the use of ZnO in the nano-size scale incorporated in membranes is a promising and novel system that may be the solution for the development of low-cost and fouling-prevention membrane technology.

The novelty of this paper is the synthesis and the incorporation of ZnO aerogel nanoparticles in polyamide membranes in order to enhance the performances of the membrane in terms of permeation, rejection and fouling resistance. The eventual membrane structure was also studied in this work.

2. Experimental

2.1 Synthesis of ZnO nanoparticles.

ZnO nanocrystals were prepared by the sol–gel method using 16 g of zinc acetate dehydrate as precursor in a 112 ml of methanol. After 15 min magnetic stirring, the solution was placed in an autoclave and dried under supercritical conditions of ethyl alcohol (EtOH).

2.2 Preparation of the nanocomposite membranes

The polyamide TFC membrane was synthesized by immersing PS-20 (polysulfone supports) in an aqueous solution of 2% MPD (1,3-Phenylendiamine, > 99%) for 2 min (the excess MPD solution was removed by rubber roller) followed by immersing the membrane in 0.1% TMC (1,3,5-benzenetricarbonyl trichloride, > 98%)/hexane (99%) solution for 1 min, then rinsed with 0.2% Na_2CO_3 after that washed with DI water, finally stored in refrigerator ≈ 4°C in DI water till use. The Nanocomposite membranes were blended with synthesized ZnO aerogel nanoparticles in a wide range of concentrations from ultralow to high (0.05-0.9 wt%) in the TMC/hexane solution. The dispersion was enhanced by sonication for 1 h.

2.3 Characterization

The crystalline phases of the obtained nanopowder were identified by X-ray diffraction (XRD) using a Bruker D5005 powder X-ray diffractometer. Transmission electron microscopy (TEM, JEM-200CX) were used to study the morphology and particle size of the powder. The specimens for TEM were prepared by putting the as-grown products in EtOH and immersing them in an ultrasonic bath for 15 min, then dropping a few drops of the resulting suspension containing the synthesized materials onto TEM grid. The morphology and microstructure of the as-synthesized nanocomposite membrane was examined by means of scanning electron microscope (SEM, FEI Nova-Nano SEM-600, Netherlands). The quantitative analysis of the membranes was performed by the mean of energy-dispersive X-ray spectroscope (EDX). In addition, atomic force microscopy (AFM) was used to analyze the surface morphology and roughness of the prepared membranes. The AFM device was Nanosurf scanning probe-optical microscope (Bruker Corporation). Small squares of the prepared membranes (approximately 1 cm^2) were cut and glued on glass substrate.

Contact angle analysis was performed using a Ramé-Hart Model 250 Standard Goniometer/ Tensiometer with DROP image advanced software (Ramé-Hart Instrument Co., Succasunna, NJ 07876 USA). A water droplet was placed on a dry flat homogeneous membrane surface and the contact angle between the water and membrane was measured until no further change was observed. The average contact angle for distilled water was determined in a series of 8 measurements for each of the different membrane surfaces. The performance of the prepared membranes was analyzed through a cross-flow system (CF042SS316 Cell, Sterlitech Corp.). The valid membrane area in this system was 42 cm^2. The feed temperature was 25°C with pH adjusted between 6 and 7. The filtration was carried out at the pressure of 225 psi and the stirring speed of 2000 rpm. All measurements of the water flux and salt rejection were measured after 30 min of water filtration experiments to ensure that had reached stability. The flux was calculated with Eq. (1)

$$J = \frac{V_p}{A \times t} \tag{1}$$

where J is the water flux (L/m^2h), Vp is the permeate volume (L), A is the membrane area (m^2) and t is the treatment time (h).

The salt rejection was measured by Eq. (2)

$$R = \left(1 - \frac{C_p}{C_f}\right) \times 100 \tag{2}$$

where R is the rejection ratio, C_p and C_f were the salt concentrations of permeate and feed, respectively.

3. Results and discussion

3.1 Characterization of the synthesized ZnO nanoparticles

The prepared ZnO nanoparticles were characterized by XRD, MET and HRMET. Fig. 1 shows typical XRD spectra of the ZnO nanoparticles aerogel after thermal treatment. We noticed the appearance of nine pronounced diffraction peaks at 2θ = 31.82°, 34.61°, 36.36°, 47.55°, 56.73°, 62.88°, 66.34°, 68.08° and 69.19° which can be attributed to the (100), (002), (101), (102) (110), (103), (200), (112) and (201) planes of ZnO, respectively (El Ghoul *et al*. 2012a and b, Krithiga and Chandrasekaran 2009). Due to the small size of the crystallites in the aerogel, the diffraction lines are broadened and are further found to depend on the Miller indices of the corresponding sets of crystal planes. For our samples, the (002) diffraction line is always narrower than the (101) line and the latter is narrower than the (100) line. This indicated an asymmetry in the crystallite shape.

The average grain size can be calculated using the Debye-Sherrer equation (Cullity 1978)

$$G = \frac{0.9\lambda}{B\cos\theta_B} \tag{3}$$

where λ is the X-ray wavelength (1.5418 Å), θB is the maximum of the Bragg diffraction peak and B is the linewidth at half maximum. After a correction for the instrumental broadening, the

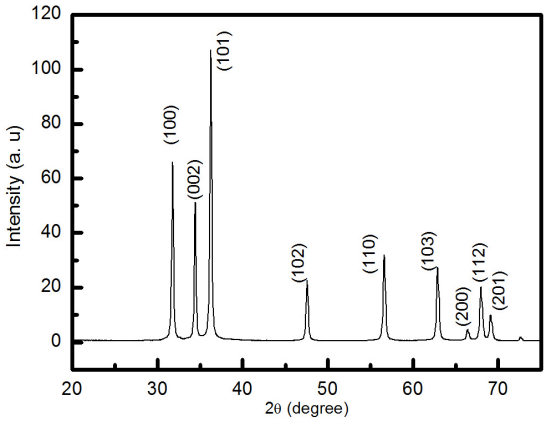

Fig. 1 XRD patterns of nanoparticles ZnO (nano-ZnO)

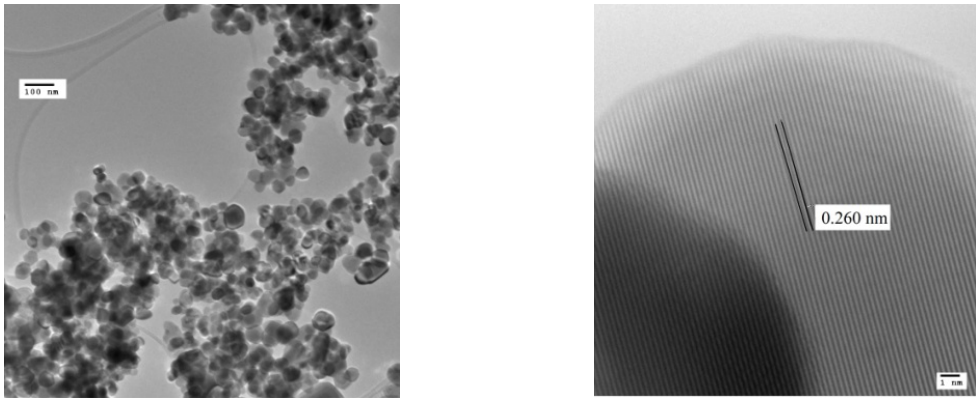

(a) (b)

Fig. 2 HR-TEM images of nanoparticles ZnO

obtained average value of the crystallites is 25 nm.

Fig. 2. shows the TEM and HRTEM images for ZnO nanoparticles. It can be seen that the samples are nearly spherical with the diameters ranging from 18 to 30 nm, which is in agreement with XRD results. HRTEM image showed that the measured distance between the planes is around 0.260 nm, which is corresponding to the (002) planes of the wurtzite ZnO.

3.2 Membranes characterizations

Membrane surfaces synthesized were observed with scanning electron microscopy (SEM) coupled with EDX analysis. Fig. 3(a) shows that the PS support layer was porous with a nanometric pore size.

After the IP process, the TFC membranes layer coated on the PS support layer by the reaction between MPD and TMC has led to a leaf-like morphology (Fig. 3(b)). The impregnation of ZnO-NPs does not have a great effect on the overall morphology of TFC in the tested concentration range, but partial aggregation of ZnO-NPs was observed in samples (Fig. 3(c)).

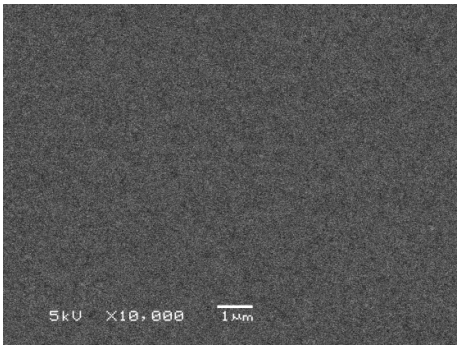

(a) PS support layer

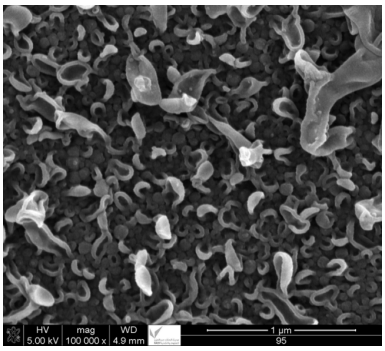

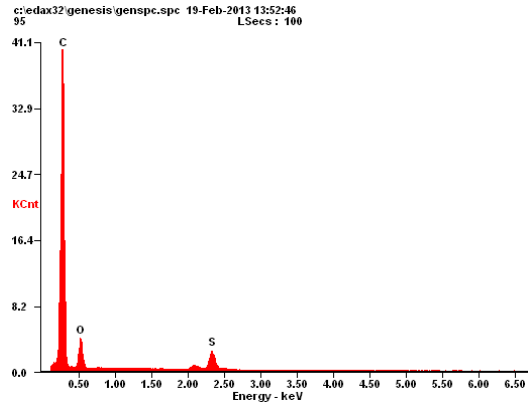

(b) TFC

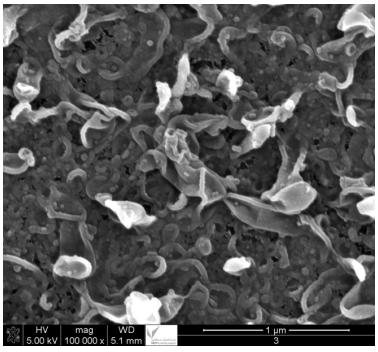

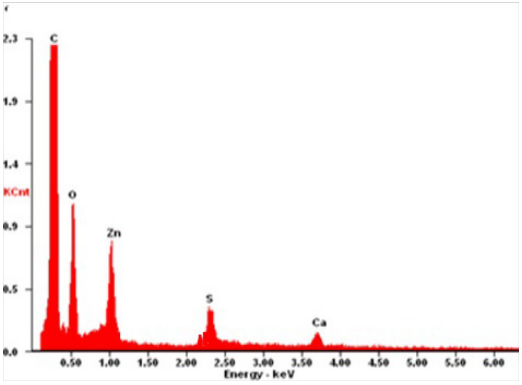

(c) TFNC-0.001

Fig. 3 EDX and SEM images of membrane surface morphologies

The difference between the images indicates clearly the presence of ZnO nanoparticles. The nano-ZnO exhibited a better dispersion in the nano-ZnO/TFC hybrid membrane as shown in Fig. 3(c), indicating the effectiveness of the dispersion process applied in membrane fabrication. This was further confirmed by EDX quantitative analysis which shows clearly the presence of carbon and oxygen with zinc peaks as component elements.

We have used the AFM to further analyze the morphology of membrane surface. As shown in Fig. 4 the TFC membrane showed much higher surface roughness (31 nm) due to the leaf-like shape of the PS support, consistent with the SEM observation (Fig. 3(a)). The RMS value increased to 68 nm in the TFNC-0.9 membrane, which could be caused by the aggregation of ZnO-NPs on the membrane surface.

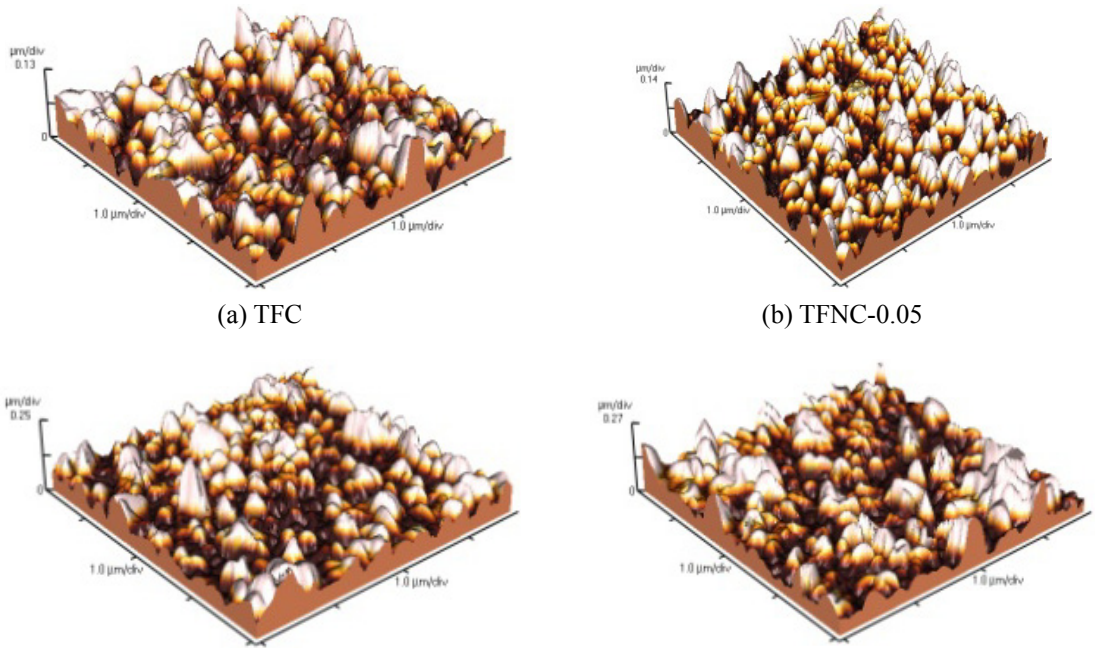

(a) TFC (b) TFNC-0.05

(c) TFNC-0.1 (d) TFNC-0.9

Fig. 4 AFM images of TFC and TFNC membranes

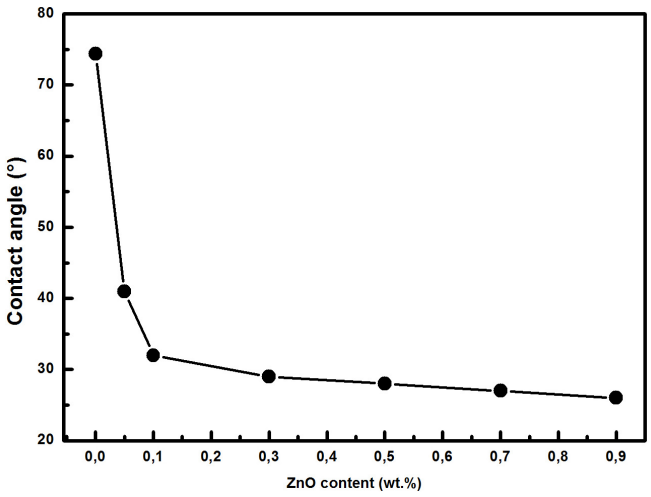

Fig. 5 Contact angle changes as the increasing concentration of added nano-ZnO

Our membranes were subjected to contact angle measurements. Standard deviations obtained on a single sample are of the order of a few degrees, which represent an acceptable reproducibility. Fig. 5 shows measurements of the contact angle for the various weights of ZnO nanoparticles. The remarkable conclusion from Fig. 5 is that even at ultra-low concentration (0.1 wt%) of embedding ZnO nanoparticles into TFC membrane, the contact angle drop significantly from 74° (control TFC membrane) to about 32°. In contrast, the hydrophilicity did not change significantly, in spite of the increasing content of ZnO nanoparticles. It is known that there is a strong correlation between the orientation (geometry) of water at a solid-liquid interface and the hydrophilicity of the solid surface (Hurwitz *et al*. 2010, Tian and shen 2009). The restructuring of interfacial water molecules can explain the increase of the hydrophilicity. The increased ordering of the interfacial water molecules improves the water molecule's ability to form hydrogen bonds and, in turn, produces stronger interactions between water and the solid phase (TFC surface).

The decrease of the contact angles in the presence of the ZnO-NPs could be caused by two reasons. First, the embedded spherical ZnO-NPs can be exposed on the membrane surface. Therefore, due to the hydrophilic properties of these NPs, the membrane surface hydrophilicity may increase. After embedding with ZnO NPs, the membrane surface could even become more hydrophilic due to the capability of the hydrophilic pores to imbibe water via capillary effects (Li *et al*. 2009). This result is in accordance with the work conducted by Jeong *et al*. (2007), which has shown that the contact angle of the membrane surface decreased with increasing Zeolite concentration and attributed this to the super-hydrophilic property of Zeolite. Second, the presence of the nanoparticles can improve the hydration and release of heat when contacting with MPD aqueous solution (Lind *et al*. 2009). This process may affect the IP reaction between MPD and TMC, and subsequently the effect on the chemical structure of the PS support. In the case where more number of the acyl chloride groups in TMC remained on the surface without reaction with amine groups, the hydrolysis of acyl chloride could generate carboxylic acid functional groups; thus, surface hydrophilicity increased (Kim *et al*. 2000). Hydrophilic nano-ZnO significantly improves the hydrophilicity of the membranes. It is known that the hydrophilic character is supportive to improve the antifouling and water flow capacity.

It has been shown that the structure and hydrophilicity of the membrane are the two main factors that govern the filtration properties of membranes. The presence of hydrophilic nano-ZnO improves the hydrophilicity of membranes, which is much favorable to the water flux. Consequently, improved hydrophilicity and advantageous membrane structure contribute to higher water flux of hybrid membrane than that of TFC membrane (Wu *et al*. 2010). The filtration properties of membranes have been obtained using the cross-flow system at 25°C. Fig. 6 shows the water fluxes and the salt rejection of all the prepared membranes. The water fluxes of all hybrid membranes are higher than that of the TFC membrane. We noticed a growth of flux when we add the nanoparticles, this flux decreases slightly after the achievement of an optimum value. The ZnO/TFC hybrid membrane exhibits the highest water flux (49 L/m^2h) when the content of added nano-ZnO is 0.1 wt%. This flux represents an improvement of 90% over that of the TFC membrane. When the concentration of added nano-ZnO exceeds 0.1 wt%, the water flux begins to decrease. This phenomenon is the synergetic result of decreased porosity and aggregation of nano-ZnO. The salt passage ratio of all prepared membranes was varied between 1 and 3%, showing a minimal value corresponding to the ultra-low concentration (0.1wt%) of the added nano-ZnO. In parallel, permeate flux and salt rejection also depend on the polyamide layer density, which is influenced by, for example, crosslink density (Song *et al*. 2005). The polymer density across the barrier layer is not uniform (Mitchell *et al*. 2011). The core layer (near the original

MPD/TMC interface) is the densest region, and the polymer density decreases gradually as the polymer grows further into the organic phase (Freger 2003, Pacheco *et al*. 2010). In many applications of interfacial polymerization using MPD and TMC, the initial amine concentration is much higher than the acyl chloride concentration. Either decreasing the amine concentration or increasing the acyl chloride concentration (thereby bringing the molar ratio of amine to acid chloride groups closer to unity) results in a denser polyamide layer compared to those prepared using higher amine/acid chloride molar ratios (Berezkin and Khokhlov 2006). Increases in either the density or thickness of the MPD/TMC barrier layer should increase the mass transfer resistance of the resulting membrane, thereby reducing permeate flux. Thus, varying the initial concentration of monomers can influence the membrane's water and salt transport properties.

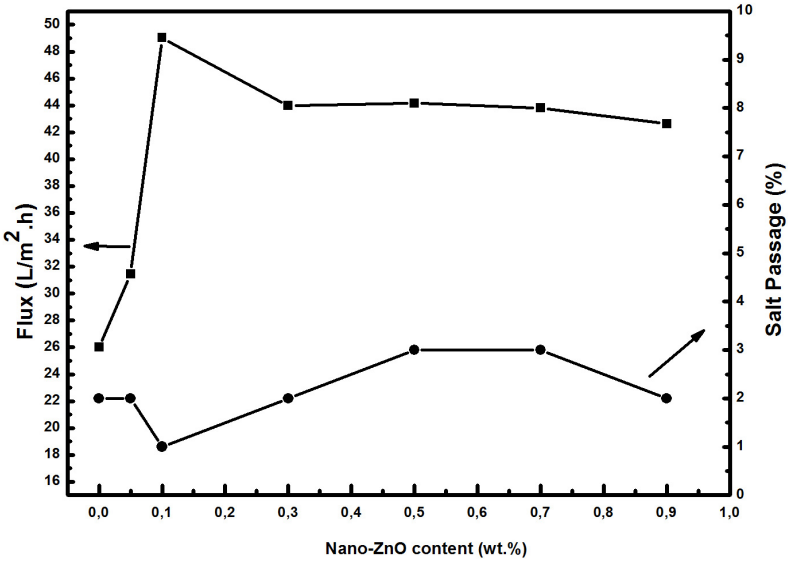

Fig. 6 Flux and rejection change as the increasing concentration of added nano-ZnO

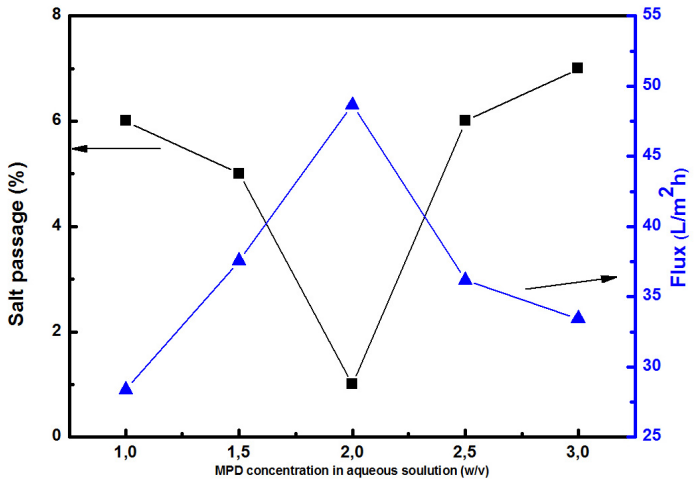

Fig. 7 Dependence of polyamide TFC membrane performance on MPD concentration

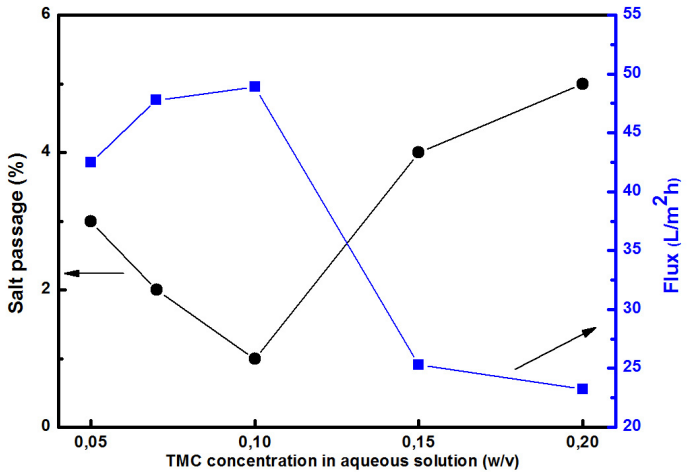

Fig. 8 Dependence of polyamide TFC membrane performance on TMC concentration

TFNC membranes were prepared by varying the concentration of MPD and TMC and keeping the concentration of added ZnO at 0.1wt%. The influence of MPD and TMC concentrations on permeate flux and salt passage is presented in Figs. 7 and 8, respectively.

To assist in the discussion below, the molar ratio of amine groups on the MPD to the acid chloride (i.e., acyl chloride) groups on the TMC, based on the concentrations of MPD and TMC used in the polymerization process is reported in these figures as well. All membranes exhibited salt passage values of less than 3% (i.e., rejection > 97%), but permeate flux varied significantly. Fig. 7 shows the influence of MPD concentration on permeate flux and salt passage. Salt passage was relatively insensitive to MPD concentration over the range of concentrations considered, suggesting the formation of defect-free (or at least nearly defect-free) membranes in all cases. Permeate flux exhibited a maximum near 2% (w/v) MPD. As MPD concentration increases, the driving force for MPD diffusion into the organic phase increases; increased MPD concentration could, therefore, increase the barrier layer thickness and, thus, lower permeate flux. As MPD concentration decreases, layer thickness is expected to decrease, which would tend to increase flux, but the resulting layer is expected to become more dense as the molar ratio of amine/acyl chloride becomes closer to unity, which would lower flux (Freger 2003, Freger and Srebnik 2003). Based on what is potentially a complex interplay between these phenomena, a maximum in permeate flux was observed. Fig. 8 illustrates the influence of TMC concentration in the organic phase on permeate flux and salt passage when the MPD concentration in the aqueous phase was held constant at 2% (w/v), which is near the optimum value observed in Fig. 7. Since interfacial polymerization is typically MPD-diffusion controlled during growth of the polyamide layer, variations in TMC concentration would affect the layer density by varying the amine/acyl chloride molar ratio (Freger 2003, Freger and Srebnik 2003). As TMC concentration increases, the amine/acyl chloride molar ratio decreases, which is expected to increase film density, resulting in lower permeate flux (Freger 2003, Freger and Srebnik 2003). However, a decrease in permeate flux was also observed at the lowest TMC concentration considered. At low TMC concentration (< 0.1%), the interfacial polymerization reaction is reported to be TMC diffusion limited (Chai and Krantz 1994). A low concentration of acyl chloride groups in the reaction zone may allow the polyamide film to grow thicker, which would decrease flux (Lind *et al*. 2009).

4. Conclusions

ZnO nanoparticles were synthesized via sol-gel method, and characterized by X-ray diffractometer and transmission electron microscope. The as synthesized NPs were embedded, with different proportions, into polyamide membrane via interfacial polymerization process. The NPs strongly affects the properties of the membrane. SEM and EDX confirm the formation of polyamide membrane embedded with zinc oxide nanoparticles. With increased proportion of added nano-ZnO, the contact angle continuously decreases. The contact angle of the membrane decreases from 74° to 32° when the content of NPs is 0.1wt%. The water flux of TFNC membrane is improved by the addition of NPs. The TFNC hybrid membrane exhibits the highest water flux (49 L/m^2h) when the content of added NPs is 0.1wt%; this flux represents an improvement of 90% relative to that of the TFC membrane. The salt passage ratio of all prepared membranes was varied between 1 and 3%, showing a minimal value corresponding to the 0.1wt% of the added nano-ZnO.

References

Berardis, B., Civitelli, G., Condello, M., Lista, P., Pozzi, R., Arancia, G. and Meschini, S. (2010), "Exposure to ZnO nanoparticles induces oxidative stress and cytotoxicity in human colon carcinoma cells", *Toxicol. Appl. Pharm.*, **246**(3), 116-127.

Berezkin, A.V. and Khokhlov, A.R. (2006), "Mathematical modeling of interfacial polycondensation", *J. Polym. Sci. B: Polym. Phys.*, **44**(18), 2698-2724.

Bottino, A., Capannelli, G. and Comite, A. (2000), "Preparation and characterization of Novel porous PVDFe ZrO_2 composite membranes", *Desalination*, **146**(1-3), 35-40.

Chai, G.Y. and Krantz, W.B. (1994), "Formation and characterization of polyamide membranes via interfacial polymerization", *J. Membr. Sci.*, **93**(2), 175-192.

Cornelius, C. Hibshman, C. and Marand, E. (2001), "Hybrid organic–inorganic membranes", *Sep. Purif. Technol.*, **25**(1-3), 181-193.

Cullity, B.D. (1978), *Elements of X-ray Diffractions*, Addison-Wesley, Reading, MA, USA, pp. 102-110.

El Ghoul, J., Barthou, C. and El Mir, L. (2012a), "Synthesis by sol-gel process, structural and optical properties of nanoparticles of zinc oxide doped vanadium", *Superlatt. Microstruct.*, **51**(6), 942-951.

El Ghoul, J., Barthou, C. and El Mir, L. (2012b), "Synthesis, structural and optical properties of nanocrystalline vanadium doped zinc oxide aerogel", *Physica E: Low-dimensional Syst. Nanostruct.*, **44**(9), 1910-1915.

El Ghoul, J., Bouguila, N., Gómez-Lopera, S.A. and El Mir, L. (2013), "Structural and optical properties of nanoparticles (V, Al) co-doped ZnO synthesized by sol-gel processes", *Superlatt. Microstruct.*, **64**, 451-459.

Franklin, N., Rogers, N.J., Apte, S.C., Batley, G.E., Gadd, G.E. and Casey, P.S. (2007), "Comparative toxicity of nanoparticulate ZnO, Bulk ZnO, and $ZnCl_2$ to a freshwater microalga (Pseudokirchneriella subcapitata): The importance of particle solubility", *Environ. Sci. Technol.*, **41**(24), 8484-8490.

Freger, V. (2003), "Nanoscale heterogeneity of polyamide membranes formed by interfacial polymerization", *Langmuir*, **19**(11), 4791-4797.

Freger, V. and Srebnik, S. (2003), "Mathematical model of charge and density distributions in interfacial polymerization of thin films", *J. Appl. Polym. Sci.*, **88**(5), 1162-1169.

Hu, W., Shiyan, C., Zhou, B. and Wang, H. (2010), "Facile synthesis of ZnO nanoparticles based on bacterial cellulose", *Mater. Sci. Eng. B*, **170**(1-3), 88-92.

Hurwitz, G., Guillen, G.R. and Hoek, E.M.V. (2010), "Probing polyamide membrane surface charge, zeta potential, wettability and hydrophilicity with cobalt contact angle measurements", *J. Membr. Sci.*, **349**(1-2), 349-357.

Jadav, G.L. and Singh, P.S. (2009), "Synthesis of novel silica polyamide nanocomposite membrane with

enhanced properties", *J. Membr. Sci*., **328**(1-2), 257-267.
Jeong, B.H., Hoek, E.M.V., Yan, Y., Subramani, A., Huang, X., Hurwitz, G., Ghosh, A.K. and Jawor, A. (2007), "Interfacial polymerization of thin film nanocomposites: A new concept for reverse osmosis membranes", *J. Membr. Sci*., **294**(1-2), 1-7.
Kim, C.K., Kim, J.H., Roh, I.J. and Kim, J.J. (2000), "The changes of membrane performance with polyamide molecular structure in the reverse osmosis process", *J. Membr. Sci*., **165**(2), 189-199.
Krithiga, R. and Chandrasekaran, G. (2009), "Synthesis, structural and optical of vanadium doped zinc oxide nanograins", *J. Crystal Growth*, **311**, 4610-4614.
Kwak, S.Y., Kim, S.H. and Kim, S.S. (2001), "Hybrid organic/inorganic reverse osmosis (RO) membrane for bactericidal anti-fouling. 1. Preparation and characterization of TiO_2 nanoparticle self-assembled aromatic polyamide thin-film-composite (TFC) membrane", *Env. Sci. Tech*., **35**, 2388-2394.
Lee, S.H.S., Im, J., Kim, J.H., Kim, H.J., Kim, J.P. and Min, B.R. (2008), "Polyamide thin-film nanofiltration membranes containing TiO_2 nanoparticles", *Desalination*, **219**(1-3), 48-56.
Li, J.H., Xu, Y.Y., Zhu, L.P., Wang, J.H. and Du, C.H. (2009), "Fabrication and characterization of a novel TiO_2 nanoparticle self-assembly membrane with improved fouling resistance", *J. Membr. Sci*., **326**(2), 659-666.
Lind, M.L., Ghosh, A.K., Jawor, A., Huang, X., Hou, W., Yang, Y. and Hoek, E.M.V. (2009), "Influence of zeolite crystal size on zeolite-polyamide thin film nanocomposite membranes", *Langmuir*, **25**(17), 10139-10145.
Liu, F., Abed, M.R.M. and Li, K. (2011), "Preparation and characterization of poly(vinylidene fluoride) (PVDF) based ultrafiltration membranes using nano gamma-Al_2O_3", *J. Membr. Sci*., **366**(1-2), 97-103.
Mercy, A.P., Upendra, N. and Ramamurthy, N. (2014), "Acoustically-enhanced particle dispersion in polystyrene/alumina nanocomposites", *Adv. Nano Res., Int. J*., **2**(2), 121-133.
Mitchell, G.E., Mickols, B., Hernandez-Cruz, D. and Hitchcock, A. (2011), "Unexpected new phase detected in FT30 type reverse osmosis membranes using scanning transmission X-ray microscopy", *Polymer*, **52**(18), 3956-3962.
Omri, K., El Ghoul, J., Lemine, O.M., Bououdina, M., Zhang, B. and El Mir, L. (2013), "Magnetic and optical properties of manganese doped ZnO nanoparticles synthesized by sol-gel technique", *Superlatt. Microstruct*., **60**, 139-147.
Pacheco, F.A., Pinnau, I., Reinhard, M. and Leckie, J.O. (2010), "Characterization of isolated polyamide thin films of RO and NF membranes using novel TEM techniques", *J. Membr. Sci*., **358**(1-2), 51-59.
Petersen, R.J. (1993), "Composite reverse-osmosis and nanofiltration membranes", *J. Membr. Sci*., **83**(1), 81-150.
Saleh, T.A. and Gupta, V.K. (2012), "Synthesis and characterization of alumina nano-particles polyamide membrane with enhanced flux rejection performance", *Sep. Purif. Technol*., **89**, 245-251.
Song, Y.J., Sun, P., Henry, L.L. and Sun, B.H. (2005), "Mechanisms of structure and performance controlled thin film composite membrane formation via interfacial polymerization process", *J. Membr. Sci*., **251**(1-2), 67-79.
Song, W., Zhang, J., Guo, J., Zhang, J., Ding, F., Li, L. and Sun, Z. (2010), "Role of the dissolved zinc ion and reactive oxygen species in cytotoxicity of ZnO nanoparticles", *Toxicol. Lett*., **199**(3), 389-397.
Sotto, A., Boromand, A., Balta, S., Darvishmanash, S., Kim, J.H., Van der Bruggen, B. (2011), "Nanofiltraiton membranes enhanced with TiO_2 nanoparticles: A comprehenisve study", *Desal. Water Treat*., **340**(1-3), 179-183.
Tian, C.S. and Shen, Y.R. (2009), "Structure and charging of hydrophobic material/water interfaces studied by phase-sensitive sum-frequency vibrational spectroscopy", *Proceedings of National Academy of Sciences of the United States of America*, **106**(36), 15148-15153.
Vaishali, K., Gunjan, K., Ramdoss, S. and Balaprasad, A. (2014), "Synthesis of defective anisotropic polyaniline/silver nanocomposites", *Adv. Nano Res., Int. J*., **2**(2), 111-119.
Wang, X.O., Li, X.Y. and Shih, K. (2011), "In situ embedment and growth of anhydrous and hydrated aluminum oxide particles on polyvinylidene fluoride (PVDF) membranes", *J. Membr. Sci*., **368**(1-2), 134-143.

Wilf, M. (2007), *The Guidebook of Membrane Desalination Technology*, Balaban Desalination Publications, Italy.

Wu, H., Tang, B. and Wu, P. (2010), "Novel ultrafiltration membranes prepared from a multiwalled carbon nanotubes/polymer composite", *J. Membr. Sci.*, **362**(1-2), 374-383.

Xie, W., Geise, G.M., Freeman, B.D., Lee, H.-S., Byun, G. and McGrath, J.E. (2012), "Polyamide interfacial composite membranes prepared from m-phenylene diamine, trimesoyl chloride and a new disulfonated diamine", *J. Membr. Sci.*, **403-404**, 152-161.

Yuan, J.H., Chen, Y., Zha, H.X., Song, L.J., Li, C.Y., Li, J.Q. and Xia, X.H. (2010), "Determination, characterization and cytotoxicity on HELF cells of ZnO nanoparticles", *Colloids Surf. B*, **76**(1), 145-150.

CC